Proceedings of the ASME 2018 International Mechanical Engineering Congress and Exposition
IMECE2018
November 9-15, 2018, Pittsburgh, Pennsylvania, USA

IMECE2018-88033

AN IMPROVED ANALYTICAL MODEL OF FRICTION AND BALL MOTION IN LINEAR BALL BEARINGS – WITH APPLICATION TO BALL-TO-BALL CONTACT PREDICTION

Bo Lin
Department of Mechanical Engineering
University of Michigan, Ann Arbor, MI, USA
bolin@umich.edu

Molong Duan
Department of Mechanical Engineering
University of Michigan, Ann Arbor, MI, USA
molong@umich.edu

Chinedum E. Okwudire
Department of Mechanical Engineering
University of Michigan, Ann Arbor, MI, USA
okwudire@umich.edu

Jason S. Wou
Ford Motor Company
Dearborn, MI, USA
swou@ford.com

ABSTRACT

The friction behavior of rolling ball machine components like linear ball bearings is very important to their functionality. For instance, differences in linear velocity of balls induces ball-to-ball contact in certain circumstances, resulting in significant increases and variations in friction. In this paper, an improved analytical formula for determining the linear velocity of balls in four-point-contact linear ball bearings is derived as a function of contact angle deviations and contact forces. The analytical formula is validated against a comprehensive friction model in the literature and shown to be in good agreement, while an oversimplified analytical model proposed by the authors in prior work is shown to be inaccurate. A case study is presented where insights gained from the derived analytical formula are used to mitigate velocity difference of balls in a linear ball bearing which otherwise would experience ball-to-ball contact.

1. INTRODUCTION

Rolling element machine components with balls, such as rotary and linear ball bearings and ball screws, are commonly used in various kinds of machinery to transmit motion with low friction [1]. They are often designed with four-point contact between ball and raceways because it offers increased rigidity and load capacity in a compact configuration [2]. Typically, four-point contact is achieved by placing oversized balls in Gothic-arch-type grooves or by using split raceways [2].

Friction of ball bearings and ball screws is very important to their functionality, such as accuracy, motion smoothness and service life [1,2]. Friction is dependent upon many factors, e.g., contact slip between balls and raceways, retainer/cage drag force, and lubrication [2]. Contact slip caused by ball-to-ball contact is the main contributor to friction increase and variation of rolling ball machine elements [3,4]. Shimoda and Izawa [3] found that friction torque in an oscillatory ball screw can be more than twice larger than usual, due to ball-to-ball contact. Ohta et al. [4], by observing loaded balls in the ball track of a linear ball bearing with a camera, proved that significant increases of friction force occur due to ball-to-ball contact.

To better understand friction, ball motion, and, by extension, issues like ball-to-ball contact in rolling ball machine components, comprehensive friction models have been developed in the literature. Pioneering work on this topic was done by Jones [5], who derived the kinematics of balls and calculated friction in two-point-contact ball bearings. Leblanc and Nelias [6], Halpin and Tran [2] followed Jones' derivation and extended his friction model to four-point-contact ball bearings. The aforementioned friction models, and many more [7,8] in the literature, usually require numerical iterations to determine friction and ball motion. The typical solution process is: first, ball motion is assumed; then, the relative velocity field between ball and raceways is established over the contact area. Accordingly, the total frictional force and moment are obtained by integrating infinitesimal frictional stress as a function of the velocity field and contact stress distribution over the contact area. Finally, quasi-static equilibrium of frictional force and moment is established for each ball to back-solve the assumed ball motion through an iterative process until the solution converges. Similar comprehensive numerical models for friction of ball screws have also been developed [9,10]. Though comprehensive, such iterative numerical solutions could be

 Copyright © 2018 by ASME

computationally expensive and do not yield general insights. For instance, they do not explicitly show how bearing parameters influence friction, ball motion and, by extension, ball-to-ball contact.

As an alternative to comprehensive models, simplified analytical models which give insights about the relationships between friction or ball motion and bearing parameters is desired. The present authors proposed a simplified analytical model for rolling/sliding friction and ball motion of four-point contact, based on point contact assumptions [11]. The simplified model explicitly captured the effects of geometric errors and misalignment on friction in analytical formulas, which is very helpful for the analysis and design optimization of ball bearings. However, the assumption of point contact oversimplifies the model [11], thus significantly diminishing its accuracy. The key contribution of this paper is, therefore, in deriving a more-accurate analytical formula for ball linear velocity in four-point-contact linear ball bearings as a function of contact angle deviations and contact forces. In deriving the analytical formula, a planar contact area is assumed, and the resulting expression for frictional force is linearized. The analytical formula for ball linear velocity is shown to be in good agreement with a comprehensive model, while the oversimplified formula derived in Ref. [11] is shown to be grossly inaccurate. Insights gained from the improved formula are useful for the analysis and design optimization of four-point-contact rolling ball machine elements, e.g., to mitigate ball-to-ball contact as shown in a case study.

The paper is organized as follows: in Section 2, the kinematics of four-point-contact linear ball bearings is introduced. The improved analytical formula for linear velocity of balls is then derived, based on a planar contact area assumption and a linear approximation of frictional force. Section 3 validates the derived analytical formula against a comprehensive friction model from the literature, followed by a case study that demonstrates ball-to-ball contact due to velocity difference of balls. By using the insights gained from the improved analytical formula, ball-to-ball contact is shown to be mitigated. Finally, conclusions and future work are presented in Section 4.

2. BALL MOTION IN FOUR-POINT CONTACT

Without loss of generality, ball motion analysis is presented in the basic module of a four-point-contact linear ball bearing as shown in Fig. 1. The analysis can be generalized to rotary ball bearing and ball screw applications with necessary modifications. In the setup, the bottom groove is fixed and the top groove is moving at a constant velocity of magnitude v. In order to obtain ball motion, friction needs to be modeled. Friction rising from ball-raceway contact is considered in this work, and it is represented by a constant sliding friction coefficient μ for metal-to-metal contact. The hydrodynamics of lubricant and gyroscopic moment are excluded in this study. The same modeling procedure (summarized in the Introduction) adopted by the comprehensive friction models [2,5–8] is followed in this section, but proper approximations made after analysis of friction lead to an explicit analytical formula for ball linear velocity.

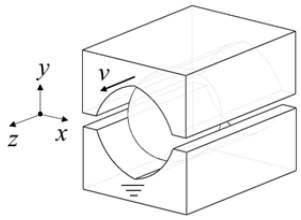

Figure 1. Basic module of four-point contact in a linear ball bearing

2.1. Kinematics of Four-point Contact

To analyze ball motion and friction, coordinate systems need to be established. Figure 2 depicts the cross section of the one-ball module shown in Fig. 1. Define a global coordinate system (CS=$\{x,y,z\}$), fixed in space with its z-axis passing through ball center and its xy-plane parallel to the cross section. A ball, with radius R_B, is in four-point contact with the BL, BR, TR and TL (representing Bottom/Top and Left/Right) grooves. Contact angles β_{BL}, β_{BR}, β_{TR} and β_{TL} are measured from $\pm y$-axis to the corresponding contact centers in the cross section (see Fig. 2). It is worth noting that contact angles are calculated a priori together with normal contact forces F_{BL}, F_{BR}, F_{TR} and F_{TL} via static load distribution models such as Ref. [12]. Local coordinate systems CS_{BL}, CS_{BR}, CS_{TR} and CS_{TL} are established at the corresponding contact centers such that local z-axes are parallel to global z-axis and local y-axes point to the origin of global coordinate system CS as shown in Fig. 2. In the authors' prior work [11], contact areas are represented as contact points to simplify the analysis. In reality, each contact area is spread over each of the ball-raceway contact interface. Since the contact area is relatively small compared to the ball radius, the contact area is assumed to be in the local xz-plane (e.g., x_{BL}-z_{BL}) in this work as shown in Fig. 2.

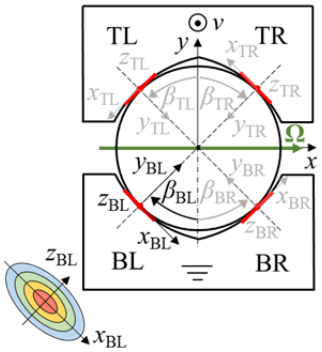

Figure 2. Geometry and coordinate systems for four-point contact

The movement of the top groove in the global z-direction at constant velocity v makes the ball to translate and rotate. Assume at quasi-static state, the ball translates with linear velocity v_B in the global z-direction (i.e., $\mathbf{v}_B=\{0, 0, v_B\}^T$ in vector form) and rotates with $\boldsymbol{\Omega}$ ($=\{\omega_x, \omega_y, \omega_z\}^T$) about an axis passing through the ball center. Velocities of any point in the contact area on both ball side and groove side can be expressed based on rigid body kinematics. Focusing on the BL contact area, $\mathbf{q}_{BL}$

Copyright © 2018 by ASME

is defined as the vector from the ball center to the BL contact center and is given in global coordinate system CS as

$$\mathbf{q}_{\mathrm{BL}}=\begin{Bmatrix}-R_{\mathrm{B}}\sin\beta_{\mathrm{BL}}\\-R_{\mathrm{B}}\cos\beta_{\mathrm{BL}}\\0\end{Bmatrix} \tag{1}$$

For any point with local coordinates $(x_{\mathrm{BL}}, z_{\mathrm{BL}})^{\mathrm{T}}$ in the contact area, its position in global coordinate system is

$$\mathbf{q}_{\mathrm{BL,B}}=\mathbf{q}_{\mathrm{BL}}+\mathbf{T}_{\mathrm{CS\text{-}CS_{BL}}}\left\{x_{\mathrm{BL}},0,z_{\mathrm{BL}}\right\}^{\mathrm{T}} \tag{2}$$

where $\mathbf{T}_{\mathrm{CS\text{-}CS_{BL}}}$ is the transformation matrix from $\mathrm{CS_{BL}}$ to CS given by

$$\mathbf{T}_{\mathrm{CS\text{-}CS_{BL}}}=\begin{bmatrix}\cos\beta_{\mathrm{BL}} & \sin\beta_{\mathrm{BL}} & 0\\-\sin\beta_{\mathrm{BL}} & \cos\beta_{\mathrm{BL}} & 0\\0 & 0 & 1\end{bmatrix} \tag{3}$$

The linear velocity at the BL contact area on the ball side in CS can be expressed as

$$\mathbf{v}_{\mathrm{BL,B}}=\boldsymbol{\Omega}\times\mathbf{q}_{\mathrm{BL,B}}+\mathbf{v}_{\mathrm{B}} \tag{4}$$

Since the bottom groove is fixed, the linear velocity at the BL contact area on the groove side is zero. Thus the relative velocity at any point in the BL contact area is

$$\Delta\mathbf{v}_{\mathrm{BL,B}}=\mathbf{v}_{\mathrm{BL,B}}-\mathbf{0}=\mathbf{v}_{\mathrm{BL,B}} \tag{5}$$

The relative velocity expressed in the contact plane (xz-plane of local coordinate system $\mathrm{CS_{BL}}$) can be formulated as

$$\begin{aligned}\begin{Bmatrix}\left(\Delta\mathbf{v}_{\mathrm{BL,B}}\right)_{\mathrm{BL},x}\\\left(\Delta\mathbf{v}_{\mathrm{BL,B}}\right)_{\mathrm{BL},z}\end{Bmatrix}&=\begin{bmatrix}1&0&0\\0&0&1\end{bmatrix}\mathbf{T}^{\mathrm{T}}_{\mathrm{CS\text{-}CS_{BL}}}\Delta\mathbf{v}_{\mathrm{BL,B}}\\&=\begin{Bmatrix}\omega_z R_{\mathrm{B}}+\left(\omega_x\sin\beta_{\mathrm{BL}}+\omega_y\cos\beta_{\mathrm{BL}}\right)z_{\mathrm{BL}}\\v_{\mathrm{B}}-\left(\omega_x\cos\beta_{\mathrm{BL}}-\omega_y\sin\beta_{\mathrm{BL}}\right)R_{\mathrm{B}}-\left(\omega_x\sin\beta_{\mathrm{BL}}+\omega_y\cos\beta_{\mathrm{BL}}\right)x_{\mathrm{BL}}\end{Bmatrix}\end{aligned} \tag{6}$$

Let

$$\begin{aligned}\omega_{\mathrm{BL}}&:=\omega_x\sin\beta_{\mathrm{BL}}+\omega_y\cos\beta_{\mathrm{BL}},\\c_{\mathrm{BL}}&:=\frac{v_{\mathrm{B}}-\left(\omega_x\cos\beta_{\mathrm{BL}}-\omega_y\sin\beta_{\mathrm{BL}}\right)R_{\mathrm{B}}}{\omega_{\mathrm{BL}}},\\d_{\mathrm{BL}}&:=-\frac{\omega_z R_{\mathrm{B}}}{\omega_{\mathrm{BL}}}\end{aligned} \tag{7}$$

The relative velocity field in Eq. (6) in the BL contact plane is rewritten as

$$\begin{Bmatrix}\left(\Delta\mathbf{v}_{\mathrm{BL,B}}\right)_{\mathrm{BL},x}\\\left(\Delta\mathbf{v}_{\mathrm{BL,B}}\right)_{\mathrm{BL},z}\end{Bmatrix}=\begin{Bmatrix}\omega_{\mathrm{BL}}\left(-d_{\mathrm{BL}}+z_{\mathrm{BL}}\right)\\\omega_{\mathrm{BL}}\left(c_{\mathrm{BL}}-z_{\mathrm{BL}}\right)\end{Bmatrix} \tag{8}$$

Following the same procedure, the velocity field for other contact areas can also be derived as

$$\begin{aligned}&\begin{Bmatrix}\left(\Delta\mathbf{v}_{\mathrm{BR,B}}\right)_{\mathrm{BR},x}\\\left(\Delta\mathbf{v}_{\mathrm{BR,B}}\right)_{\mathrm{BR},z}\end{Bmatrix}=\begin{Bmatrix}\omega_{\mathrm{BR}}\left(-d_{\mathrm{BR}}+z_{\mathrm{BR}}\right)\\\omega_{\mathrm{BR}}\left(c_{\mathrm{BR}}-x_{\mathrm{BR}}\right)\end{Bmatrix}\\&=\begin{Bmatrix}\omega_z R_{\mathrm{B}}+\left(-\omega_x\sin\beta_{\mathrm{BR}}+\omega_y\cos\beta_{\mathrm{BR}}\right)z_{\mathrm{BR}}\\v_{\mathrm{B}}-\left(\omega_x\cos\beta_{\mathrm{BR}}+\omega_y\sin\beta_{\mathrm{BR}}\right)R_{\mathrm{B}}-\left(-\omega_x\sin\beta_{\mathrm{BR}}+\omega_y\cos\beta_{\mathrm{BR}}\right)x_{\mathrm{BR}}\end{Bmatrix},\\&\begin{Bmatrix}\left(\Delta\mathbf{v}_{\mathrm{TR,B}}\right)_{\mathrm{TR},x}\\\left(\Delta\mathbf{v}_{\mathrm{TR,B}}\right)_{\mathrm{TR},z}\end{Bmatrix}=\begin{Bmatrix}\omega_{\mathrm{TR}}\left(-d_{\mathrm{TR}}+z_{\mathrm{TR}}\right)\\\omega_{\mathrm{TR}}\left(c_{\mathrm{TR}}-x_{\mathrm{TR}}\right)\end{Bmatrix}\\&=\begin{Bmatrix}\omega_z R_{\mathrm{B}}+\left(-\omega_x\sin\beta_{\mathrm{TR}}-\omega_y\cos\beta_{\mathrm{TR}}\right)z_{\mathrm{TR}}\\v_{\mathrm{B}}-v+\left(\omega_x\cos\beta_{\mathrm{TR}}-\omega_y\sin\beta_{\mathrm{TR}}\right)R_{\mathrm{B}}-\left(-\omega_x\sin\beta_{\mathrm{TR}}-\omega_y\cos\beta_{\mathrm{TR}}\right)x_{\mathrm{TR}}\end{Bmatrix},\\&\begin{Bmatrix}\left(\Delta\mathbf{v}_{\mathrm{TL,B}}\right)_{\mathrm{TL},x}\\\left(\Delta\mathbf{v}_{\mathrm{TL,B}}\right)_{\mathrm{TL},z}\end{Bmatrix}=\begin{Bmatrix}\omega_{\mathrm{TL}}\left(-d_{\mathrm{TL}}+z_{\mathrm{TL}}\right)\\\omega_{\mathrm{TL}}\left(c_{\mathrm{TL}}-x_{\mathrm{TL}}\right)\end{Bmatrix}\\&=\begin{Bmatrix}\omega_z R_{\mathrm{B}}+\left(\omega_x\sin\beta_{\mathrm{TL}}-\omega_y\cos\beta_{\mathrm{TL}}\right)z_{\mathrm{TL}}\\v_{\mathrm{B}}-v+\left(\omega_x\cos\beta_{\mathrm{TL}}+\omega_y\sin\beta_{\mathrm{TL}}\right)R_{\mathrm{B}}-\left(\omega_x\sin\beta_{\mathrm{TL}}-\omega_y\cos\beta_{\mathrm{TL}}\right)x_{\mathrm{TL}}\end{Bmatrix}\end{aligned} \tag{9}$$

It is observed that the relative velocity field in the elliptical contact area (with semi-major axis a_i and semi-minor axis b_i) is a circular contour centered at (c_i, d_i) as shown in Fig. 3(a), with $i\in\{\mathrm{BL,BR,TR,TL}\}$ representing different contact area. Notice that the center of the contour represents the zero-velocity point. Another observation about the velocity field in Eqs. (6) and (9) is that the offset in the x_i-component (local x-component) are all $\omega_z R_{\mathrm{B}}$, which is induced by the rotation of ball around the global z-axis. It can be proved that the same offset gives rise to frictional forces in all positive or all negative local x-direction for all four contact points if $\omega_z\neq 0$. In that case, frictional moment about global z-axis is non-zero, which is not feasible in the quasi-static state. In order for the quasi-static state to hold, $\omega_z=0$ has to be enforced. Thus $d_i=0$ as shown in Fig. 3(b) is the case for all four contact points in linear ball bearings.

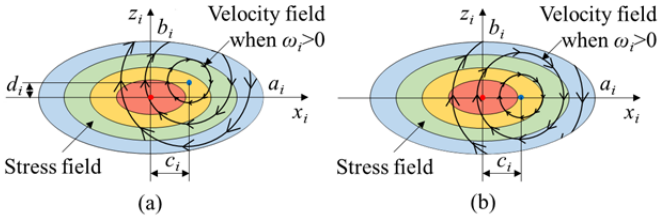

Figure 3. Contact area and velocity field: (a) when $\omega_z\neq 0$; (b) linear ball bearing case where $\omega_z=0$ is enforced

From now on, the discussion will be only focused on the case $d_i=0$, where velocity center is always on the semi-major axis of the elliptical contact area. The velocity field for the four contact areas in Eqs. (8) and (9) are represented by a common formula as

$$\begin{Bmatrix}\left(\Delta\mathbf{v}_{i,\mathrm{B}}\right)_{i,x}\\\left(\Delta\mathbf{v}_{i,\mathrm{B}}\right)_{i,z}\end{Bmatrix}=\begin{Bmatrix}\omega_i z_i\\\omega_i\left(c_i-x_i\right)\end{Bmatrix},i\in\left\{\mathrm{BL,BR,TR,TL}\right\} \tag{10}$$

It is worth noting that derivation of velocity field in the contact area for ball bearing was done in many comprehensive friction models in the literature [2,5–8]. However, with contact plane

Copyright © 2018 by ASME

approximation in this work, a neat expression of velocity field is obtained and its circular contour pattern is found, which is very helpful for the analysis of friction.

2.2. Frictional Force and Moment in the Contact Area

Now that the velocity field is expressed over the assumed planar contact area, friction can be calculated given normal contact stress distribution. This is a standard process that Jones and other researchers adopted [2,5–8]. But with the velocity field derived in last subsection, friction can be analyzed explicitly. The normal contact stress field indicated by the color map in Fig. 3 is described by Hertzian Contact Theory as

$$\sigma_i = \sigma_{i,0}\left(1-\frac{x_i^2}{a_i^2}-\frac{z_i^2}{b_i^2}\right)^{1/2},\ \sigma_{i,0}=\frac{3F_i}{2\pi a_i b_i} \tag{11}$$

where a_i and b_i are determined given the contact surface geometry and normal contact force F_i for each contact area, the details of which are shown in Ref. [13]. Given the symmetry of the contact stress field and velocity field about the x_i-axis in Fig. 3(a), the frictional force along x_i-axis is zero. The frictional force along z_i-axis and frictional moment about contact center are calculated by double integrating the frictional stress over the contact area as

$$\begin{aligned} f_{i,z} &= \mathrm{sgn}(\omega_i)\iint_D \mu\sigma_i \frac{x_i-c_i}{\sqrt{(x_i-c_i)^2+y_i^2}}dx_i dy_i \\ &= \mathrm{sgn}(\omega_i)a_i b_i \mu\sigma_{i,0}\iint_D \left(1-t^2-s^2\right)^{1/2}\frac{t-c_i/a_i}{\sqrt{(t-c_i/a_i)^2+(b_i/a_i\cdot s-d_i/a_i)^2}}dsdt \quad \left(t=\frac{x_i}{a_i}, s=\frac{y_i}{b_i}, D: t^2+s^2\le 1\right) \\ &= \mathrm{sgn}(\omega_i)a_i b_i \mu\sigma_{i,0}\int_0^{2\pi}\int_0^1 \left(1-r^2\right)^{1/2}\frac{r\cos\theta-c_i/a_i}{\sqrt{(r\cos\theta-c_i/a_i)^2+(b_i/a_i\cdot r\sin\theta-d_i/a_i)^2}}rdrd\theta \ (t=r\cos\theta, s=r\sin\theta) \end{aligned} \tag{12}$$

$$\begin{aligned} M_{i,O} &= \mathrm{sgn}(\omega_i)\iint_D \mu\sigma_{i,0}\left(1-\frac{x_i^2}{a_i^2}-\frac{y_i^2}{b_i^2}\right)^{1/2}\left(\frac{x_i-c_i}{\sqrt{(x_i-c_i)^2+y_i^2}}x_i-\frac{-y_i}{\sqrt{(x_i-c_i)^2+y_i^2}}y_i\right)dxdy \\ &= \mathrm{sgn}(\omega_i)a_i^2 b_i \mu\sigma_{i,0}\iint_D \left(1-t^2-s^2\right)^{1/2}\left(\frac{t^2-c_i/a_i t+b_i^2/a_i^2 s^2}{\sqrt{(t-c_i/a_i)^2+(b_i/a_i\cdot s)^2}}\right)dsdt \quad \left(t=\frac{x_i}{a_i}, s=\frac{y_i}{b_i}, D: t^2+s^2\le 1\right) \\ &= \mathrm{sgn}(\omega_i)a_i^2 b_i \mu\sigma_{i,0}\int_0^{2\pi}\int_0^1 \left(1-r^2\right)^{1/2}\left(\frac{r^2\cos\theta^2-c_i/a_i\, r\cos\theta+b_i^2/a_i^2\, r^2\sin\theta^2}{\sqrt{(r\cos\theta-c_i/a_i)^2+(b_i/a_i\cdot r\sin\theta)^2}}\right)rdrd\theta \ (t=r\cos\theta, s=r\sin\theta) \end{aligned} \tag{13}$$

The frictional force and moment are functions of c_i/a_i, an indicator for the deviation of velocity center from contact center. Extreme values of $f_{i,z}$ and $M_{i,O}$ are achieved at $c_i/a_i=0$ as

$$f_{i,z}\big|_{c_i/a_i=0}=0,$$
$$M_{i,O}\big|_{c_i/a_i=0}=\frac{3}{8}\mathrm{sgn}(\omega_i)\mu F_i a_i\cdot\mathrm{Ellip}\left(\frac{\sqrt{a_i^2-b_i^2}}{a_i}\right) \tag{14}$$

where Ellip(·) represents the complete elliptic integral of the second kind. The case of $c_i/a_i=0$ represents pure spin. The other set of extreme values are achieved when $c_i/a_i\to\pm\infty$ as

$$\begin{aligned} f_{i,z}\big|_{c_i/a_i\to\pm\infty} &= \mp\mathrm{sgn}(\omega_i)\mu F_i, \\ M_{i,O}\big|_{c_i/a_i=\pm\infty} &= 0 \end{aligned} \tag{15}$$

where pure sliding happens.

2.3. Approximation of Frictional Force and Moment

The frictional force and moment expressed in Eqs. (12) and (13) are affected by b_i/a_i, which is the same for four contact points in a linear ball bearing and is solely determined by the conformity ratio of the groove [2,6] (i.e., conf. = $R_G/2R_B$, with R_G representing the radius of the groove). There is no explicit expression for the double integral of the frictional force and moment in Eqs. (12) and (13). However, Fig. 4 shows the numerical results of normalized $f_{i,z}$ and $M_{i,O}$ as functions of c_i/a_i under four typical conformity ratios of bearings [6]. To normalize $f_{i,z}$, it is divided by its extreme value $\mathrm{sgn}(\omega_i)\mu F_i$; while $M_{i,O}$ is normalized by dividing $\mathrm{sgn}(\omega_i)\mu F_i$ and moment arm R_B in order to make it comparable in magnitude to $f_{i,z}$ in the force and moment equilibrium equation.

Observing from Fig. 4, there is no significant difference among the plots of the four typical conformity ratios, thus they will not be distinguished in this work. It is observed that the normalized frictional moment is very small compared to the normalized frictional force over a wide range as shown in Fig. 4(a). Frictional moment is only comparable to frictional force when c_i/a_i is very close to zero. When $|c_i/a_i|<0.5$, $f_{i,z}$ is almost linear with respect to c_i/a_i as shown in Fig. 4(b). While in the same region, the change of normalized $M_{i,O}$ is negligible compared to that of $f_{i,z}$. In fact, $|c_i/a_i|$ is usually very small in

Copyright © 2018 by ASME

four-point contact as observed from the results presented in Ref. [6,14]. Small $|c_i/a_i|$ condition breaks down only when there is two-point contact or near two-point contact (i.e., contact forces on one diagonal pair are significantly larger than those on the other pair). Thus to simplify the analysis for four-point contact, frictional force is approximated to be linear with respect to c_i/a_i while frictional moment is approximated to always take its maximum value given in Eq. (14).

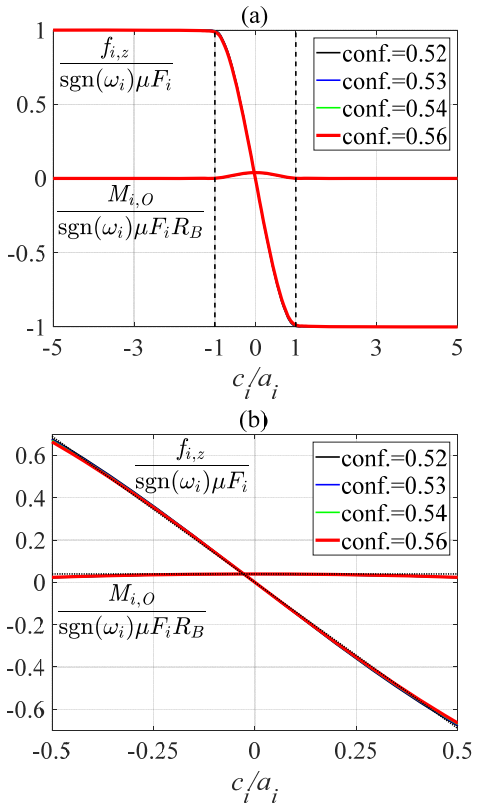

Figure 4. Frictional force and moment as functions of c_i/a_i: (a) full plot; (b) zoomed in plot near $c_i/a_i = 0$

To aid the analysis, an additional variable $\Delta\gamma_i$ is introduced for each contact area (see Fig. 5), indicating the angular deviation of the velocity center from contact center in the cross section (i.e., along semi-major axis of the contact area). Thus

$$\Delta\gamma_i = \frac{c_i}{R_B} \tag{16}$$

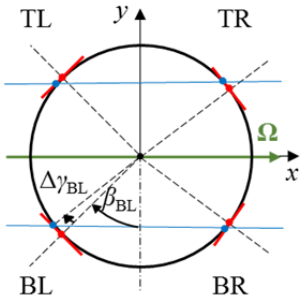

Figure 5. Angular deviation of velocity center from contact center

In accordance with small c_i/a_i assumption, $\Delta\gamma_i$ is even smaller. With linear approximation, frictional force becomes

$$f_{i,z} = \mathrm{sgn}(\omega_i)\mu F_i k_f \frac{c_i}{a_i} = \mathrm{sgn}(\omega_i)\mu F_i k_f \frac{R_B}{a_i}\Delta\gamma_i \tag{17}$$

Based on the plot in Fig. 4, k_f=−1.38 is picked.

The ball needs to be in quasi-static equilibrium under frictional force and moment as

$$\begin{bmatrix} 1 & 1 & 1 & 1 \\ -\cos\beta_{BL} & -\cos\beta_{BR} & \cos\beta_{TR} & \cos\beta_{TL} \\ \sin\beta_{BL} & -\sin\beta_{BR} & -\sin\beta_{TR} & \sin\beta_{TL} \end{bmatrix} \begin{Bmatrix} f_{BL,z} \\ f_{BR,z} \\ f_{TR,z} \\ f_{TL,z} \end{Bmatrix} + \begin{bmatrix} 0 & 0 & 0 & 0 \\ \sin\beta_{BL} & -\sin\beta_{BR} & -\sin\beta_{TR} & \sin\beta_{TL} \\ \cos\beta_{BL} & \cos\beta_{BR} & -\cos\beta_{TR} & -\cos\beta_{TL} \end{bmatrix} \begin{Bmatrix} M_{BL,O}/R_B \\ M_{BR,O}/R_B \\ M_{TR,O}/R_B \\ M_{TL,O}/R_B \end{Bmatrix} = \begin{Bmatrix} 0 \\ 0 \\ 0 \end{Bmatrix} \tag{18}$$

Besides equilibrium of frictional force and moment, one more relationship comes from the kinematic constraint. In the authors' prior work [11], it is found that the two "zero-velocity lines" that pass through the zero-velocity points on the same side of the groove (see blue lines in Fig. 5) are parallel. It still holds true in this work with $\beta_i+\Delta\gamma_i$ representing the angle of velocity center. This means

$$\begin{aligned} &\sin(\beta_{BL}+\Delta\gamma_{BL}+\beta_{TL}+\Delta\gamma_{TL})+\sin(\beta_{BR}+\Delta\gamma_{BR}-\beta_{TL}-\Delta\gamma_{TL}) \\ &=\sin(\beta_{BR}+\Delta\gamma_{BR}+\beta_{TR}+\Delta\gamma_{TR})+\sin(\beta_{BL}+\Delta\gamma_{BL}-\beta_{TR}-\Delta\gamma_{TR}) \end{aligned} \tag{19}$$

For contact angles β_i, there is a nominal value β_0. However, the actual contact angle deviates from β_0 due to the presence of geometric error and/or misalignment. Define

$$\Delta\beta_i := \beta_i - \beta_0 \tag{20}$$

where $\Delta\beta_i$ is the contact angle deviation and is usually very small (typically $-3°<\Delta\beta_i<3°$).

Under the assumption of small $\Delta\beta_i+\Delta\gamma_i$, Eq. (18) is approximated as

$$\begin{bmatrix} 1 & -1 & -1 & 1 \end{bmatrix} \begin{Bmatrix} \Delta\gamma_{BL} \\ \Delta\gamma_{BR} \\ \Delta\gamma_{TR} \\ \Delta\gamma_{TL} \end{Bmatrix} + (\Delta\beta_{BL}+\Delta\beta_{TL}-\Delta\beta_{BR}-\Delta\beta_{TR}) = 0 \tag{21}$$

Putting Eqs.(17)(18)(21) together, the angular deviation $\Delta\gamma_i$ are analytically solved using Matlab Symbolic Toolbox.

2.4. Effect of Contact Angle Deviation on Ball Motion

The effect of contact angle deviations on ball linear velocity is of particular interest in this work. From prior work [11], the linear velocity of ball center is formulated as

$$\begin{aligned} &v_B = \frac{\sin(\hat{\beta}_{BL}+\hat{\beta}_{BR})v}{\sin(\hat{\beta}_{BL}+\hat{\beta}_{BR})+\sin(\hat{\beta}_{BL}+\hat{\beta}_{TL})+\sin(\hat{\beta}_{BR}-\hat{\beta}_{TL})}, \\ &\hat{\beta}_{BL}=\beta_{BL}+\Delta\gamma_{BL}, \hat{\beta}_{BR}=\beta_{BR}+\Delta\gamma_{BR}, \\ &\hat{\beta}_{TR}=\beta_{TR}+\Delta\gamma_{TR}, \hat{\beta}_{TL}=\beta_{TL}+\Delta\gamma_{TL} \end{aligned} \tag{22}$$

Copyright © 2018 by ASME

With small $\Delta\beta_i+\Delta\gamma_i$ approximation, Eq. (22) reduces to

$$v_B \approx \underbrace{\left(1+\left(1-\cos\left(2\beta_0\right)\right)\frac{-\Delta\beta_{BR}-\Delta\gamma_{BR}+\Delta\beta_{TL}+\Delta\gamma_{TL}}{2}\right)}_{\varepsilon}\frac{v}{2} \tag{23}$$

where ε is the deviation of ball center velocity from the nominal ball center velocity $v/2$. Substitute the solution of $\Delta\gamma_i$ obtained in last subsection into Eq. (23), ε is obtained as a function of four contact angle deviation $\Delta\beta_i$ and four normal contact forces F_i. Since contact angle deviation $\Delta\beta_i$ is small, the contact forces on the same diagonal pair (i.e., BL and TR pair, BR and TL pair) are very close under external loading [14]. With approximation that $F_{BL}\approx F_{TR}\approx F_1$ and $F_{BR}\approx F_{TL}\approx F_2$, the ball center velocity deviation is simplified to be

$$\varepsilon\approx\left(1-\cos\left(2\beta_0\right)\right)\frac{\left(-\Delta\beta_{BL}+\Delta\beta_{TR}\right)F_1^{2/3}+\left(-\Delta\beta_{BR}+\Delta\beta_{TL}\right)F_2^{2/3}}{2\left(F_1^{2/3}+F_2^{2/3}\right)} \tag{24}$$

This formula shows the effect of contact angle deviations and contact forces on the ball linear velocity deviation ε. A few insights obtained from the formula for ε are: (1) ball velocity is not affected by external loading in the absence of contact angle deviation; (2) given the same contact angle deviations, the ball center velocity deviation will be different under different loading condition; (3) if $-\Delta\beta_{BL}+\Delta\beta_{TR} = -\Delta\beta_{BR}+\Delta\beta_{TL}$, then Eq. (24) reduces to

$$\varepsilon\approx\left(1-\cos\left(2\beta_0\right)\right)\frac{-\Delta\beta_{BL}+\Delta\beta_{TR}}{2} \tag{25}$$

which is independent on external loading condition. These insights are helpful for design optimization of four-point-contact linear ball bearings to reduce velocity difference of balls as will be shown in Section 3.

Compared to the comprehensive friction models in the literature, three approximations are made in the derivation: (I) planar contact area is assumed; (II) $\Delta\beta_i+\Delta\gamma_i$ for each contact point is small; (III) contact forces on the same diagonal pair are approximated to be the same. Four-point contact is a necessary condition for approximation (II). If there are only two contact points or near two-point contact (i.e., contact forces on one diagonal pair are significantly larger than those on the other pair), the angular deviation of velocity center from contact center $\Delta\gamma_i$ becomes large so that small $\Delta\beta_i+\Delta\gamma_i$ assumption becomes invalid.

3. VALIDATION AND CASE STUDIES

In the preceding section, an analytical formula for ball linear velocity in four-point contact is derived with approximations. In this section, the derived analytical formula is validated against a comprehensive friction model in the literature. Results from the authors' prior work are also compared to show the improvement made in this work. A case study is presented to demonstrate ball-to-ball contact due to velocity difference of balls induced by contact angle deviations. By using the insights gained from the derived analytical formula, ball-to-ball contact is shown to be mitigated.

3.1. Validation of the Derived Analytical Formula

To validate the derived analytical formula of ball velocity deviation, it is compared to a comprehensive friction model in the literature in the setup as shown in Fig. 6. Without loss of generality, the nominal contact angle β_0 is set to be 45°. Contact angle deviation θ (<3°) only takes place on the bottom groove. This type of contact angle deviation can be caused by manufacturing error and/or misalignment. According to the definition of contact angle deviations in this work, $\Delta\beta_{BL}=-\theta$, $\Delta\beta_{BR}=\theta$ and $\Delta\beta_{TL}=\Delta\beta_{TR}=0$. The external loading is represented by N_x and N_y applied to the top groove. Since the contact angle deviations are small, it is reasonable to approximate the four contact forces as $F_{BL}\approx F_{TR}\approx F_1=\sqrt{2}/2(N_y-N_x)$ and $F_{BR}\approx F_{TL}\approx F_2=\sqrt{2}/2(N_y+N_x)$. Define $\rho=N_x/N_y$ as the side force ratio and substitute all these parameters into Eq. (24), the ball velocity deviation in this case study is formulated as

$$\varepsilon\approx\frac{\theta F_1^{2/3}-\theta F_2^{2/3}}{2\left(F_1^{2/3}+F_2^{2/3}\right)}=\frac{\left(1-\left(\frac{1+\rho}{1-\rho}\right)^{2/3}\right)}{\left(1+\left(\frac{1+\rho}{1-\rho}\right)^{2/3}\right)}\frac{\theta}{2} \tag{26}$$

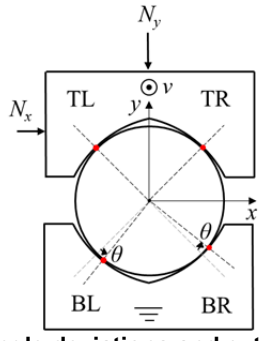

Figure 6. Contact angle deviations and external loading in the case study

As benchmark for the comparison, the comprehensive friction model is Leblanc's model with details presented in Ref. [6]. The ball velocity deviation of both the derived formula in this work and simplified model in the authors' prior work [11] is found to have explicit forms only dependent on contact angle deviation θ and side force ratio ρ. On the contrary, Leblanc's model needs to go through iterative numerical process to calculate the linear velocity of the ball. Parameters for Leblanc's model in this case study are shown in Table 1.

Table 1. Parameters for the case study

Parameter (Symbol)	Value [Unit]
Ball radius (R_B)	5 [mm]
Conformity ratio of groove (conf.)	0.54
Normal force (N_y)	200 [N]
Velocity of the top groove (v)	10 [mm/s]
Friction coefficient of metal-to-metal contact (μ)	0.1
Young's modulus	210 [N/mm^2]
Poisson's ratio	0.28

Copyright © 2018 by ASME

Figure 7 compares the ball linear velocity deviation ε from the three models under different loading ρ and contact angle deviation θ. It is observed that results from the analytical formula derived in this work (see Fig. 7(c)) match with Leblanc's models (Fig. 7(a)) closely. The difference of velocity deviation only becomes noticeable when the magnitudes of side force ratio $|\rho|$ and contact angle deviation $|\theta|$ are large as shown in Fig. 7(d). Large $|\rho|$ and $|\theta|$ are exactly where Approximation (II) summarized at the end of Section 2 fails: four-point contact tends to be two-point contact when $|\rho|$ is large, together with large $|\theta|$, the small $\Delta\beta_i+\Delta\gamma_i$ assumption is untenable. But overall, the analytical formula derived predicts the velocity deviation to a reasonable extent in four-point contact. On the other hand, the authors' prior work with point contact assumption (see Fig. 7(b)) is shown to be in gross error compared to both Lelanc's model and the derived analytical formula, because the point contact assumption is oversimplified.

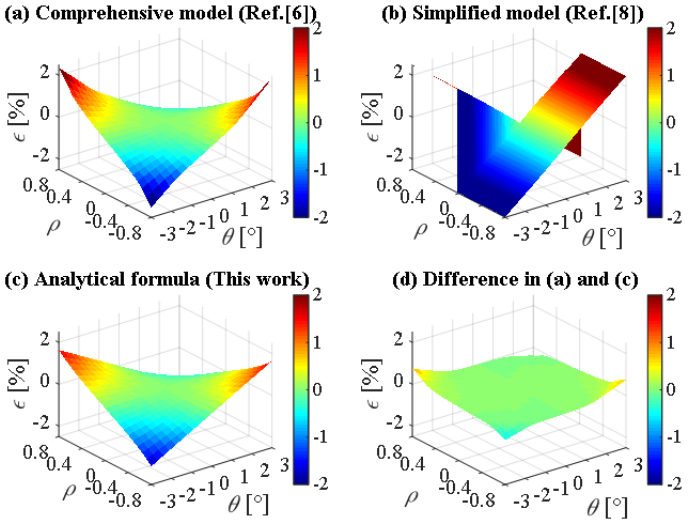

Figure 7. Comparison of velocity deviation from three models

3.2. Ball-to-ball Contact Prediction

From ball motion analysis of single balls, it is observed that contact angle deviations, under external loading, induce ball velocity deviation. When these balls are on the same track, velocity difference can result in ball-to-ball contact if the linear velocity of the ball behind is faster than the ball in front and when the two balls are close enough. Ball-to-ball contact is well-known to give rise to significant friction increase and friction variation so it is desirable to avoid or at least mitigate ball-to-ball contact.

Figure 8 shows the front view and side view of two balls on the same linear ball bearing with initial gap $\Delta d_0=0.1R_B$. The same type of contact angle deviation in Fig. 6 from last case study is assumed for the bottom groove with $\theta=2°$. Assume the same N_y is applied to Ball 1 and Ball 2 but N_x on the two balls is of opposite direction such that $\rho_1=N_{x1}/N_{y1}=-0.6$ and $\rho_2=N_{x2}/N_{y2}=0.6$. This kind of loading represents a yaw moment applied to the top groove, which accelerates ball-to-ball contact as shown in Ref. [4].

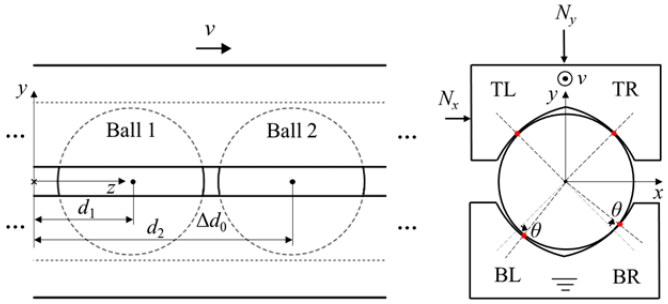

Figure 8. Setup for ball-to-ball contact and avoidance study

According to Eq. (26), the velocity deviations ε_1 and ε_2 of Ball 1 and Ball 2 respectively are different because of different ρ_1 and ρ_2. The contact angle deviations and the velocity deviations calculated from both Leblanc's model and the derived analytical formula are summarized in Table 2 as Case (a). Despite the small difference, both models predict that Ball 1 is moving faster than Ball 2. Ball location can be calculated as an integral of ball velocity. The deviation of ball location from its nominal location ($vt/2$) according to the derived analytical formula is plotted in Fig. 9(a). It is obvious that ball-to-ball contact takes place due to the velocity difference.

There are engineering solutions for mitigating ball to ball contact such as using spacer balls or cages. However, the derived analytical formula sheds light into how to mitigate ball-to-ball contact by reducing velocity difference of ball. Given the contact angle deviations on the bottom groove, if the contact angle deviations on the top groove can be controlled or manipulated in the manufacturing or assembly process, the velocity difference of balls can be minimized and ball-to-ball contact can be mitigated. From Eq. (24), it is found that if $\Delta\beta_{TR}=\Delta\beta_{BL}$ and $\Delta\beta_{TL}=\Delta\beta_{BR}$, then the velocity deviation is always zero irrespective of external loading. This optimized design is simulated with the results shown in Table 2 as Case (b) and plotted in Fig. 9(b). Although Leblanc's model (and other comprehensive friction models) is able to calculate velocity deviation of balls given contact angle deviations, it lacks the ability to make predictions and give guidelines for design optimization except by trial and error.

Table 2. Contact angle deviations and velocity deviation of balls in two cases

	Contact angle deviations ($-\Delta\beta_{BL}=\Delta\beta_{BR}=\theta=2°$)		Velocity deviation		
	$\Delta\beta_{TR}$	$\Delta\beta_{TL}$		Leblanc's model	Derived formula
Case (a)	0	0	ε_1	0.85%	0.75%
			ε_2	−0.77%	−0.75%
Case (b)	$-\theta$	θ	ε_1	0	0
			ε_2	0	0

Copyright © 2018 by ASME

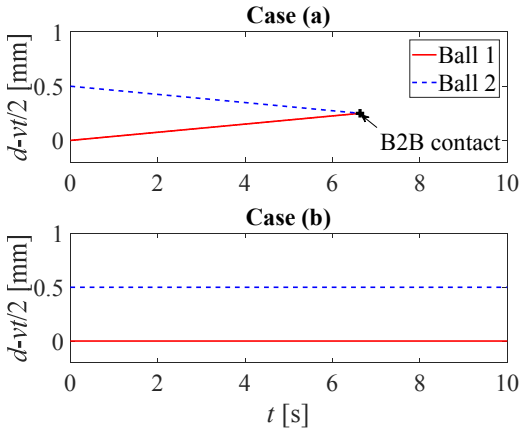

Figure 9. Example of ball-to-ball contact and avoidance

4. CONCLUSION AND FUTURE WORK

Friction behavior is very important to rolling ball machine components like linear ball bearings. Difference in linear velocity of balls, resulting from contact angle deviations, induces issues like ball-to-ball contact in certain circumstances, giving rise to significant increases and variations of friction. In this paper, an analytical formula for ball linear velocity in four-point-contact linear ball bearings is derived as a function of contact angle deviations and contact forces. It is based on two major approximations: (i) planar contact area; (ii) linearized frictional force. Thus the derived formula is valid for linear ball bearings in four-point contact with small contact angle deviations. The results of the analytical formula is compared to a comprehensive friction model in the literature and shown to be in good agreement. Ball-to-ball contact due to velocity difference of balls induced by contact angle deviations is demonstrated in a case study. Using the insights gained from the derived analytical formula, ball-to-ball contact is shown to be mitigated by reducing the velocity difference of balls. This work focuses what gives rise to velocity difference of balls that leads to ball-to-ball contact. But the effect of velocity difference on the level of ball-to-ball contact force and sliding friction loss still remains a question. It will be addressed in the future work.

REFERENCES

[1] Hong, S., and Tong, V.-C., 2016, "Rolling-Element Bearing Modeling : A Review," Int. J. Precis. Eng. Manuf., **17**(12), pp. 1729–1749.

[2] Halpin, J. D., and Tran, A. N., 2016, "An Analytical Model of Four-Point Contact Rolling Element Ball Bearings," J. Tribol., **138**(3), p. 31404.

[3] Izawa, I., and Shimoda, H., 1976, "Study on the Load Distribution in the Ball Screw-in the Case of Preloaded Ball Screw."

[4] Ohta, H., Hanaoka, G., and Ueki, Y., 2017, "Sticking of a Linear-Guideway Type Recirculating Ball Bearing," J. Tribol., **139**(3), p. 31103.

[5] Jones, A. B., 1959, "Ball Motion and Sliding Friction in Ball Bearings," J. Basic Eng., **81**(3), pp. 1–12.

[6] Leblanc, A., and Nelias, D., 2007, "Ball Motion and Sliding Friction in a Four-Contact-Point Ball Bearing," J. Tribol., **129**(4), pp. 801–808.

[7] Hamrock, B. J., 1975, "Ball Motion and Sliding Friction in an Arched Outer Race Ball Bearing," J. Lubr. Technol., **97**(2), pp. 202–210.

[8] Harris, T. A., and Kotzalas, M. N., 1980, *Advanced Concepts of Bearing Technology*, CRC Press.

[9] Wei, C. C., and Lin, J. F., 2003, "Kinematic Analysis of the Ball Screw Mechanism Considering Variable Contact Angles and Elastic Deformations," J. Mech. Des., **125**(4), p. 717.

[10] Chung, C., Fin, J., and Horng, J., 2009, "Analysis of a Ball Screw with a Preload and Lubrication," Tribiology Int., **42**(11–12), pp. 1816–1831.

[11] Lin, B., Duan, M., Okwudire, C. E., and Wou, J. S., 2018, "A Simplified Analytical Model for Rolling/Sliding Behavior and Friction in Four-Point-Contact Ball Bearings and Screws," *Proceedings of the ASME 2017 International Mechanical Engineering Congress and Exposition*, pp. 1–9.

[12] Amasorrain, J. I., Sagartzazu, X., and Damián, J., 2003, "Load Distribution in a Four Contact-Point Slewing Bearing," Mech. Mach. Theory, **38**(6), pp. 479–496.

[13] Johnson, K. L., 1985, *Contact Mechanics*, Cambridge University Press.

[14] Heras, I., Aguirrebeitia, J., Abasolo, M., and Plaza, J., 2017, "Friction Torque in Four-Point Contact Slewing Bearings : Applicability and Limitations of Current Analytical Formulations," Tribol. Int., **115**, pp. 59–69.

Copyright © 2018 by ASME